in the mixture of acetonides can be calculated by comparison of the activity of the recrystallized product with the activity of the labeled mixture of acetonides.
13. Like the yield dependence of the six linear steps (*8*), the six tandem stereoselective events are also linearly related. For earlier discussions of this latter phenomenon, see J. P. Vigneron, M. Dhaenens, A. Horeau, *Tetrahedron* **29**, 1055 (1973); T. R. Hoye and J. C. Suhadolnik, *ibid.* **42**, 2855 (1986); S. L. Schreiber, T. S. Schreiber, D. B. Smith, *J. Am. Chem. Soc.* **109**, 1525 (1987); V. Rautenstrauch, P. Mégard, B. Bourdin, A. Furrer, *ibid.* **114**, 1418 (1992).
14. The dodecaols (+)-**4** and (−)-**4** have the following spectral data. ^{1}H NMR (D$_2$O, 400 MHz): δ 3.33 (d, $J = 10.4$ Hz, 1 H), 3.23 (d, $J = 10.2$ Hz, 1 H), 3.15 (d, $J = 10.4$ Hz, 1 H), 1.65 to 1.37 (m, 8 H), 1.24 to 1.15 (m, 2 H), 1.02 (s, 6 H), 0.993 (s, 3 H), and 0.991 (s, 3 H). ^{13}C NMR (dimethyl sulfoxide-d$_6$, 100 MHz): δ 78.41, 77.92, 77.02, 73.55, 73.49, 71.75, 35.16, 35.03, 28.27, 26.27, 24.74, 24.65, 22.69, and 22.59. High-resolution mass spectrum: calculated for $C_{30}H_{62}O_{12}$ (M + Na$^+$), 637.4139; found, 637.4139. Combustion analysis: calculated for $C_{30}H_{62}O_{12}\cdot H_2O$, C, 56.94, and H, 10.19; found C, 56.59, and H, 10.00. Melting point: 195° to 198°C (decomposes). Optical rotations: $[\alpha]_D^{24.5}$ + 53.6° (c = 0.5, H$_2$O) for (+)-**4**, $[\alpha]_D^{22.5}$ − 49.0° (c = 0.5, H$_2$O) for (−)-**4**.
15. Financial support was provided by the National Institutes of Health (GM 28384) and the National Science Foundation (CHE-8903218). We thank R. Chadra for providing the x-ray crystal structure of the hexaacetonide (−)-**3** and D. Rideout for his assistance with the ^{14}C isotope dilution experiments.

15 September 1992; accepted 9 November 1992

Effect of Pressure on the Composition of the Lower Mantle End Member Fe$_x$O

Catherine McCammon

The composition limits of Fe$_x$O are sensitive to both pressure and temperature. Earlier studies have shown that Fe$_x$O becomes highly nonstoichiometric when in equilibrium with metallic iron above 10 gigapascals, which is difficult to reconcile with available thermodynamic data. Experiments with a uniaxial split-sphere apparatus demonstrate that the iron content of Fe$_x$O increases continuously at high pressure in excellent agreement with quantitative models and suggest that there is a discontinuity in the elastic properties of Fe$_x$O above $x = 0.95$. On the basis of these results, it is inferred that the Earth's present lower mantle is not in equilibrium with metallic iron.

Knowledge of the amount of Fe^{3+} in Fe$_x$O, and ultimately in (Mg,Fe)O, is of fundamental importance to studies of lower mantle properties such as electrical conductivity and oxygen fugacity (f_{O_2}). The maximum Fe content of Fe$_x$O at atmospheric pressure is limited to about $x = 0.95$, which corresponds to Fe^{3+}/ΣFe = 0.11 on the basis of electrostatic charge balance. Although studies have shown that more stoichiometric samples can be synthesized at pressures up to 10 GPa (*1–4*), experiments at higher pressures indicate that Fe$_x$O becomes significantly less stoichiometric in equilibrium with metallic Fe (*4, 5*) (Fig. 1). Although such behavior can be understood qualitatively in terms of a composition-dependent bulk modulus for Fe$_x$O, the extreme nonstoichiometry along the Fe-Fe$_x$O phase boundary at higher pressures cannot be explained (*4*). Small sample sizes have caused large uncertainties in earlier determinations of Fe-Fe$_x$O phase relations, but recent advances in high-pressure technology allow the recovery of several milligrams of sample. The wide pressure range available enables all experiments to be performed on one type of apparatus, which avoids inconsistencies resulting from different f_{O_2} conditions. In this study, I used a multianvil press to determine accurately the Fe-Fe$_x$O phase boundary at high pressure and temperature.

As described in (*4*), Fe$_{0.952}$O was prepared at atmospheric pressure in an evacuated silica glass tube, mixed with Fe powder in the molar ratio 10:1, and packed into an Fe capsule to buffer f_{O_2} conditions during the run. I performed the experiments on a 1200-T split-sphere multianvil apparatus with the use of Cr$_2$O$_3$-doped MgO octahedra as a pressure medium. In runs up to 10 GPa, I used 18-mm (edge) octahedra with a stepped graphite heater (*6*), whereas for runs from 14 to 18 GPa, I used 10-mm (edge) octahedra with a LaCrO$_3$ heater. Each run lasted 1 hour (*7*). Pressure was calibrated at room temperature with the use of transitions in Bi, ZnS, and GaS; at 1000°C with quartz-coesite and coesite-stishovite reactions (18-mm assembly); and at 1200° and 1600°C with the olivine–β-phase and β-phase–spinel transitions in Mg$_2$SiO$_4$ (10-mm assembly). Temperatures were initially measured with a W$_{75}$Re$_{25}$-W$_{97}$Re$_3$ thermocouple but, because of thermocouple failure during the compression phase of each experiment, I estimated the final temperature on the basis of a calibrated power curve derived from a minimum of three previous experiments that were carried out on the same assembly at the same pressure and temperature conditions. I performed one additional experiment on a conventional piston cylinder press. The final composition of each sample was determined by x-ray diffraction on the basis of the linear relation between cubic cell parameter and iron composition (*4*). Mössbauer spectra were recorded at both room temperature and 80 K to correlate hyperfine parameters with expected Fe^{3+} content (*8*). The Mössbauer parameters were consistent with the composition determined by x-ray diffraction.

The results of all runs (Table 1) indicate that the Fe content of Fe$_x$O in equilibrium with metallic Fe increases with pressure until reaching a plateau near Fe$_{0.98}$O. There is clearly no decrease in Fe content above 10 GPa as previously observed. Although a change in composition during the quenching process cannot be completely ruled out, the observation that the limiting composition (Fe$_{0.98}$O) was the same as earlier experimental results at 775°C (*1*) argues against such a possibility. A temperature uncertainty of ±100°C is estimated to contribute a maximum uncertainty of ±0.001 in x (*9*).

One explanation for the extremely low Fe content obtained in the earlier experiments is that Fe$_x$O is difficult to heat in diamond-anvil cell experiments because it absorbs laser radiation poorly at high pressure (*4*); thus, temperatures may have been overestimated. The γ-ε transition in Fe occurs near 780°C at 20 GPa (*10*), and temperatures lower than this boundary

Table 1. Details of high-pressure runs on Fe$_x$O in equilibrium with metallic Fe. Uncertainties are given in parentheses.

Synthesis technique	Pressure (GPa)	Temperature (°C)	Cell dimension (a) of Fe$_x$O (pm)	Fe$_x$O composition*
Evac. silica tube		1000(5)	431.09(5)	0.952(2)
Piston cylinder	1.5(5)	1000(10)	431.35(5)	0.957(2)
Multianvil press	5.0(5)	1000(50)	431.92(5)	0.969(2)
Multianvil press	10.0(5)	1000(100)	432.37(5)	0.978(2)
Multianvil press	14.0(5)	1000(100)	432.41(5)	0.979(3)
Multianvil press	18.0(5)	1000(100)	432.44(5)	0.980(2)

*Calculated from $a = 385.6 + 47.8x$ (*4*).

Bayerisches Geoinstitut, Postfach 10 12 51, W-8580 Bayreuth, Germany.

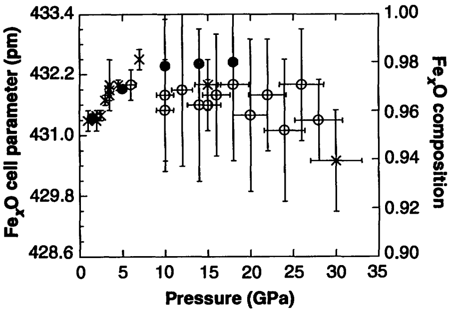

Fig. 1. Effect of pressure on the composition of Fe$_x$O in equilibrium with metallic Fe at about 1000°C. Experiments performed in large volume equipment are represented by x's (*1–4*), open circles correspond to diamond-anvil cell experiments (*4, 5*), and solid circles indicate the new data.

would favor formation of an assemblage containing Fe-deficient Fe$_x$O and ϵ-Fe because the density is higher than for Fe-rich Fe$_x$O. Another explanation is that there was insufficient Fe in earlier experiments to constrain f_{O_2} conditions to those found at Fe equilibrium (*11*).

The position of the Fe-Fe$_x$O boundary at high pressures and temperatures depends on the effect of Fe composition on the isothermal bulk modulus (K_T) of Fe$_x$O (*4*). Although the scatter of experimentally determined K_T values appears large (Fig. 2), recent work (*12*) has demonstrated that all deviations in earlier work from the range $K_T \approx 150$ to 154 GPa for $x = 0.90$ to 0.95 can be accounted for. Hazen (*13*) has shown experimentally that there is a small change of K_T from 152 to 154 GPa between Fe$_{0.90}$O and Fe$_{0.947}$O. If we assume that Hazen's K_T-x relation is valid for all Fe$_x$O compositions, the calculated value of the Fe-Fe$_x$O phase boundary asymptotically approaches the Fe$_{1.00}$O end member (Fig. 3, dotted curve). There is clearly a discrepancy between experimental and calculated curves above 10 GPa. If, however, Hazen's K_T-x relation is assumed to be valid between Fe$_{0.90}$O and Fe$_{0.95}$O, and a steeper relation between Fe$_{0.95}$O and Fe$_{1.00}$O that passes through the datapoints in Fig. 2 is assumed, the calculated phase boundary increases to 10 GPa where a plateau is reached (Fig. 3, solid curve). The second model clearly provides a better fit to my experimental data (*14*).

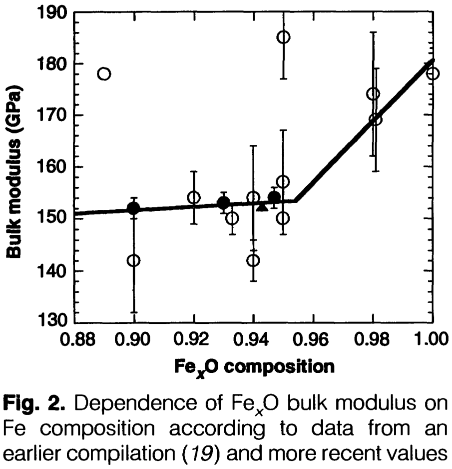

Fig. 2. Dependence of Fe$_x$O bulk modulus on Fe composition according to data from an earlier compilation (*19*) and more recent values (*16, 17, 23*). Solid circles represent results of a differential-compression experiment (*13*), the solid triangle corresponds to a recent ultrasonic study (*12*), and open circles indicate all other data. The solid line indicates the relation assumed in this study.

The K_T values for Fe$_{0.90}$O to Fe$_{0.95}$O lie in the range 150 to 154 GPa (*12*), but there are few data for compositions that are richer in Fe. Yagi *et al.* (*16*) obtained a value of 169 GPa with the pressure derivative $\partial K_T/\partial P = 4$ from compression measurements on Fe$_{0.98}$O but conceded that large errors (±10 GPa) and the tradeoff between K_T and $\partial K_T/\partial P$ prevent a definitive conclusion. Crystal field models of MnO, FeO, CoO, and NiO imply that K_T should be 178 GPa for Fe$_{1.00}$O (*12, 17*), although it is difficult to assess uncertainties in such a calculation. Although a discontinuous variation of Fe$_x$O bulk modulus with composition is consistent with available data, final confirmation must await high-quality elasticity data on the relevant compositions.

If there is a discontinuous variation of K_T with x, other properties of Fe$_x$O might be expected to show similar discontinuities. The cubic cell parameter appears to increase linearly with increasing x [see (*4*) and references therein]; however, the defect structure is not determined uniquely by the cell parameter. Mössbauer studies of Fe$_x$O with $x = 0.95$ to 0.98 have shown that there may be a change of defect structure in Fe-rich ($x > 0.95$) samples (*8*). More significantly, a recent study (*18*) of the Néel temperature (T_N) of Fe$_x$O shows that T_N decreases linearly as x increases from 0.90 to 0.95 but, from 0.95 to 0.98, there is a large discontinuity and T_N increases with x. Although these results also suggest a change in defect structure, studies of other Fe-rich Fe$_x$O properties are required to confirm the presence of such a change.

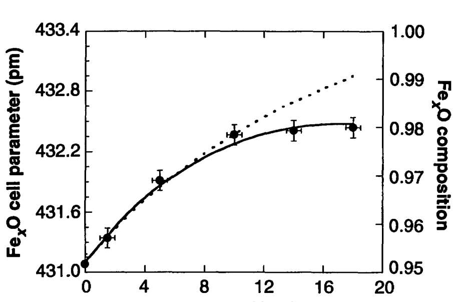

Fig. 3. Effect of pressure on the composition of Fe$_x$O in equilibrium with metallic Fe at 1000° ± 100°C from new experiments in a multianvil press. To calculate the theoretical curves, I assumed two different K_T versus x relations for Fe$_x$O: (i) linear from Fe$_{0.90}$O to Fe$_{1.00}$O (dotted line); and (ii) discontinuous linear variation illustrated in Fig. 2 (solid line).

These results show that caution must be exercised in the extrapolation of Fe$_x$O properties to high pressure. Samples of Fe$_x$O with $x < 0.95$ have traditionally been used to measure properties in the laboratory, but these are relevant only to 1 atm. At higher pressures, Fe$_x$O is richer in Fe and has different magnetic properties (*18*), as well as inferred elastic properties. Other properties, such as electrical conductivity, may also vary; therefore, experiments should be performed on samples quenched from the appropriate pressures and temperatures or measured in situ.

Knowledge of the Fe-Fe$_x$O phase diagram can be used to estimate the maximum Fe^{3+} content of (Mg,Fe)O, a likely component of the Earth's lower mantle, at lower mantle pressures and temperatures in equilibrium with metallic Fe. Experiments at atmospheric pressure have shown that Fe^{3+}/ΣFe decreases from 0.11 at the Fe$_x$O end-member to 0.02 for Mg$_{0.8}$Fe$_{0.2}$O in equilibrium with metallic Fe [see (*19*) and references therein]. The lower Fe^{3+}/ΣFe ratio results from a lowering of the minimum f_{O_2} stability boundary of (Fe,Mg)O by the addition of Mg^{2+} and, because pressure affects both phase boundaries in a similar manner (*20*), the Fe^{3+}/ΣFe ratio should always be greater for Fe$_x$O than for (Fe,Mg)O in equilibrium with metallic Fe. Experiments have confirmed that addition of Mg^{2+} reduces Fe^{3+}/ΣFe in (Fe,Mg)O at pressures up to 20 GPa (*22*). Extrapolation of my results to 1800°C and 24 GPa, conditions appropriate for the top of the Earth's lower mantle, suggests a maximum Fe^{3+}/ΣFe ratio of 0.05 for (Fe,Mg)O in equilibrium with metallic Fe (*23*). Higher pressures and temperatures favor less Fe^{3+} (*24*), so the ratio would probably decrease as pressures and temperatures increased deeper in the lower mantle. The addition of SiO$_2$ to the system is likely to decrease further the Fe^{3+} content of (Fe,Mg)O because the perovskite-Fe-stishovite buffer lies below the Fe-wüstite buffer [see, for example, (*25*)].

Measurements of the electrical conductivity of (Fe,Mg)O have shown that the value increases with Fe^{3+}/ΣFe (*26*), which suggests that lower mantle conductivity is dominated by (Fe,Mg)O (*26, 27*). Comparison with lower mantle values from geophysical data suggests a significant amount of Fe^{3+} in lower mantle (Fe,Mg)O [see, for example, (*26*)], but my results imply a low Fe^{3+} content for lower mantle (Fe,Mg)O in equilibrium with metallic Fe; therefore, it appears unlikely that the present-day lower mantle could be in equilibrium with metallic Fe.

REFERENCES AND NOTES

1. T. Katsura, B. Iwasaki, S. Kimura, S. Akimoto, *J. Chem. Phys.* **47**, 4559 (1967).
2. H. Sawamoto, E. Ohtani, M. Kumazawa, in *Proceedings of the 4th International Conference on High Pressures*, J. Osugi, Ed. (Physical Chemistry Society of Japan, Kyoto, 1974), pp. 194–201.
3. B. Simons and F. Seifert, *Carnegie Inst. Washington Yearb.* **78**, 625 (1979).
4. C. A. McCammon and L. Liu, *Phys. Chem. Miner.* **10**, 106 (1984).
5. L. Liu, *Earth Planet. Sci. Lett.* **33**, 101 (1976).
6. D. Canil, *ibid.* **106**, 64 (1991).
7. Previous experiments (*1, 4*) have demonstrated that equilibrium is achieved within this time.
8. C. A. McCammon and D. C. Price, *Phys. Chem. Miner.* **11**, 250 (1984).
9. Experiments have shown that *x* decreases by 0.002 from 920° to 1200°C at 4.5 GPa (*1*). Calculations have shown (*4*) that this difference does not increase significantly at higher pressure.
10. R. Boehler, *Geophys. Res. Lett.* **13**, 1153 (1986).
11. In particular, Sawamoto *et al.* (*2*) used a Pt capsule that also served as the heater; thus, the sample was buffered well above Fe-Fe$_x$O equilibrium.
12. I. Jackson, S. K. Khanna, A. Revcolevschi, J. Berthon, *J. Geophys. Res.* **95**, 21671 (1990).
13. R. M. Hazen, *Carnegie Inst. Washington Yearb.* **80**, 277 (1981).
14. The discrepancy could also be caused by a composition-dependent temperature effect (for example, if the thermal expansion of Fe$_x$O varied dramatically with *x* at high pressure). This possibility seems less likely, however. In my calculations, I assumed a constant thermal expansion for Fe$_x$O but, nevertheless, reproduced the temperature effect on the Fe-Fe$_x$O phase boundary observed from 775° to 1200°C up to pressures of 4.5 GPa (*1*). Also, thermal expansion of Fe$_x$O does not appear to vary with *x* at atmospheric pressure (*15*).
15. M. Hayakawa, J. B. Cohen, T. B. Reed, *J. Am. Ceram. Soc.* **55**, 160 (1972).
16. T. Yagi, T. Suzuki, S. Akimoto, *J. Geophys. Res.* **90**, 8784 (1985).
17. S. L. Webb, I. Jackson, J. D. Fitz Gerald, *Phys. Earth Planet. Inter.* **52**, 117 (1988).
18. C. A. McCammon, *J. Magn. Magn. Mater.* **104–107**, 1937 (1992).
19. R. M. Hazen and R. Jeanloz, *Rev. Geophys. Space Phys.* **22**, 37 (1984).
20. Hirsch (*21*) has calculated the effect of pressure and temperature on the Fe-Fe$_x$O buffer and showed that f_{O_2} is nearly insensitive to variation of input parameters with *x*. Because input parameters of (Fe,Mg)O are similar to those for Fe$_x$O, pressure and temperature should have a similar effect on the Fe-(Fe,Mg)O buffer.
21. L. M. Hirsch, *Geophys. Res. Lett.* **18**, 1309 (1991).
22. M. Kato, S. Urakawa, M. Kumazawa, paper presented at the DELP 1989 Misasa International Symposium and the Second Japan-USSR Symposium, Misasa, Japan, 17 to 22 April 1989.
23. Extrapolation beyond experimental-data conditions increases the uncertainty of this determination. Accordingly, I have restricted calculations to the maximum value only and allowed for uncertainties in input parameters.
24. The Fe^{3+}/ΣFe ratio decreases with increasing pressure to at least 18 GPa (Fig. 3) and, in the absence of phase transitions, this trend is unlikely to change significantly at higher pressure. The effect of temperature on the Fe-Fe$_x$O phase boundary is reduced with increasing pressure (*4*); this trend is also unlikely to change. The γ-ϵ phase transition in Fe would favor a larger Fe^{3+}/ΣFe ratio at higher pressures and lower temperatures, but the transition boundary crosses the Earth's geotherm only in the deep mantle (*10*), and the effect would be reduced in any event because of the small Fe concentration of the lower-mantle (Mg,Fe)O.
25. H. St. C. O'Neill *et al.*, in *Proceedings of IUGG Symposium U12*, E. Takahashi, R. Jeanloz, D. C. Rubie, Eds. (American Geophysical Union, Washington, DC, in press).
26. B. J. Wood and J. Nell, *Nature* **351**, 309 (1991).
27. J. Peyronneau and J. P. Poirier, *ibid.* **342**, 537 (1989); X. Li and R. Jeanloz, *J. Geophys. Res.* **95**, 21609 (1990); *ibid.* **96**, 6113 (1991).

28. I am grateful to Dr. Rubie for assistance with the multianvil experiments and to I. Jackson, D. Mao, H. O'Neill, S. Rigden, and F. Seifert for comments on the manuscript.

21 July 1992; accepted 2 November 1992

A Traveling-Wave Amplifier Model of the Cochlea

Allyn Hubbard

A two-mode model of the cochlea that uses active intermode feedback has been developed that quantitatively accounts for the motion of the basilar membrane in response to single tones and qualitatively accounts for cochlear emission phenomena. In contrast to existing single-mode models, this model amplifies the mechanical traveling wave in spatially localized cochlear regions where an approximate match occurs between the traveling-wave velocities of each of the two traveling-wave lines or modes.

The concept of a "second filter" in the mammalian cochlea was originally proposed to account for the apparent discrepancy between broadly tuned cochlear micromechanics (*1*) and highly tuned, auditory nerve responses (*2*). This concept has been abandoned in the past decade because of experiments demonstrating little difference between the tuning properties of the cochlear mechanics (*3*), the sensory receptors (*4*), and the auditory nerve fibers. This report proposes a model that matches mechanical data (*5*) extremely well and, therefore, has the potential to expand our understanding of the mechanisms underlying the unique sensitivity and frequency selectivity of the cochlea.

Cellular and extracellular structures partition the cochlea into several longitudinal, fluid-filled ducts (Fig. 1). The anatomical picture is far more complicated than classical cochlear models (*6*), which approximate the major partition between upper and lower scalae as a single membrane. The membrane was assumed to respond to the pressure difference between the scala tympani and scala vestibuli, resulting in a single vibration mode that propagates acoustic energy down the cochlea. However, in a structure like that of Fig. 1, every duct and boundary partition can support propagation modes. My model shows that we can produce realistic cochlear responses using two actively coupled modes.

The active components of this model are the cochlear outer hair cells that abut the upper and lower boundary structures in the fluid-filled outer tunnel. Depolarization of isolated outer hair cells causes a decrease in cell body length and generates forces of about 0.5 nN/mV. For voltage changes comparable to those that occur in the natural cochlear transduction process, reproduced by electrical stimulation of the cochlea, significant acoustic signals can be measured at the eardrum [see (*7*)]. Therefore, it is reasonable to believe that in vivo hair cells respond to their receptor current by changing their length, thus exerting microforces on other cochlear structures, which, in a yet unknown way, produces amplification of the mechanical traveling wave. In my model, forces are exchanged (fed back) between the transmission lines, each representing a different mode of wave propagation.

Earlier models have used local feedback (*8*), but the feedback apparatus appended to each model segment was not longitudinally connected to form an additional propagation mode. Zweig's (*9*) locally applied feedback expression was derived under the condition that the feedback cause the classical model (*6*) to fit modified experimental data. De Boer (*10*) has described possible modes in a multiple-duct model. My work demonstrates that coupling two modes with the use of feedback results in a type of traveling-wave amplifier.

Classical electronic traveling-wave amplifiers (*11*) are composed of two transmission lines connected by transistors along their lengths. The transmission lines are made up of concatenated passive components. The input signal travels along one line, providing a control signal to the transistors. The control signal causes the transistors to regulate the current supplied to the second transmission line, called the output line. The most constructive current addition occurs when the propagation velocities on both lines are equal. Thus, an ever-growing signal travels down the output

---

College of Engineering and School of Medicine, Boston University, Boston, MA 02215.